

The Air–Sea Momentum Flux in Conditions of Wind Sea and Swell

MARK A. DONELAN AND WILLIAM M. DRENNAN

National Water Research Institute, Burlington, Ontario, Canada

KRISTINA B. KATSAROS

University of Washington, Seattle, Washington

(Manuscript received 18 October 1995, in final form 16 September 1996)

ABSTRACT

During the Surface Wave Dynamics Experiment, direct measurements of momentum, heat, and water vapor fluxes were obtained from a mast on the foredeck of a SWATH (small water-plane area, twin hull) ship in deep water off the state of Virginia. Directional wave spectra were obtained simultaneously from a 6- or 3-wire wave-staff array mounted at the bow of the ship. One hundred and twenty-six 17-minute runs of flux and wave data obtained with the ship steaming slowly into the wind are examined for the effects of the relative direction of the wind sea and background swell on the momentum transfer. The adequacy of the inertial dissipation method, which depends on the high-frequency turbulent fluctuations for evaluating the wind stress, is also examined for any effects of swell.

The results show that the presence of counter- and cross-swells can result in drag coefficients that are much larger than the value for a pure wind sea. The eddy correlation and inertial dissipation methods for measuring wind stress are found to diverge during the complex sea conditions. The authors interpret the latter observations as an indication that the traditional inertial dissipation method, in which the pressure and transport terms in the kinetic energy balance equation are assumed to be in balance, may be unsuitable for use in a marine boundary layer disturbed by swell.

1. Introduction

During the past thirty years, a great deal of effort has been expended in determining the fluxes of momentum, heat, and moisture over the ocean surface. These variables are key boundary conditions for coupled atmosphere–ocean models. An understanding of how they vary with changing sea conditions is one of the most challenging goals of research in air–sea interaction. The recent development of satellite and other remote sensing systems may soon allow for fluxes to be measured over the entire global ocean. Although this goal may not be far off, several key issues remain to be addressed. For instance, the relationship between the backscatter coefficients determined by the remote sensors, momentum flux, and the varying sea state is not fully known.

The dependence of the momentum flux, or wind stress τ , on the various physical parameters governing the exchange process has long been a topic of research. We introduce the drag coefficient $C_{Dz} = \tau/\rho U_z^2$, where ρ is the air density and U_z the mean wind speed at reference

height z , usually taken to be 10 m. Many earlier studies (e.g., Smith 1980; Large and Pond 1981) concluded that C_{D10N} , the 10-m drag coefficient in neutrally stratified conditions, is a function of wind speed alone. This view, however, was not supported by the data of Donelan (1990). These fetch-limited data suggest a further dependence of C_{D10N} on wave age, with C_{D10N} increasing for younger waves due to an increased surface roughness. Subsequent support for this hypothesis has been found by Smith et al. (1992) and Donelan et al. (1993).

The presence of swell(s) is another factor that may be important in parameterizing the drag coefficient. Donelan (1987) has shown with laboratory data that the presence of long, gentle swell propagating in the wind direction has a substantial effect on the wind sea spectrum. Since the short, steep, slow moving wind sea supports the bulk of the wind stress in this situation, the swell may have a significant effect on the overall roughness. On the other hand, Dobson et al. (1994) presented shipborne inertial dissipation data of momentum flux in strong swell conditions and tested the hypothesis that by simply “deleting” the swell from the wave spectra, existing drag coefficient/wave age relations would hold. Although the statistical significance was low, they concluded that there were no extra effects from the swell. We note though that their inertial dissipation method, based on high-fre-

Corresponding author address: Dr. M. A. Donelan, Department of Applied Marine Physics, RSMAS, University of Miami, 4600 Rickenbacker Causeway, Miami, FL 33149-1098.
E-mail: mdonelan@RSMAS.Miami.edu

quency components of the wind spectrum alone (those above the wind sea peak—see below), might well be inadequate for determining the effects of much lower frequency swell.

The recent results of Nghiem et al. (1995) provide indirect support for the opposite conclusion. Their Ku- and C-band radar data show a strong increase in the backscatter coefficients in situations of light winds and strong swell. Eliminating other effects (such as wave breaking), they concluded that the likely cause of the higher values was an increase in wind stress. In this paper, we present open ocean eddy-correlation data that imply a strong dependence of C_{D10N} on swell. The dataset includes conditions of strong swell propagating against both moderate and light winds.

2. Measuring stress

In the constant stress layer, well away from the thin viscous layer at the surface, the fluxes of momentum, heat, and mass are carried by turbulent fluctuations. In this case, the wind stress is given by

$$\tau = -\rho \overline{w'u'}, \quad (1)$$

where ρ is the air density, assumed constant, and w' and u' the turbulent fluctuations in vertical and horizontal velocities. The overbar refers to averaging over a suitable time interval. Based on studies of the separation of spectral scales in boundary layer winds, Pierson (1983) determined a “suitable interval” to be one of approximately 20 minutes.

There are four methods for estimating fluxes in common use: eddy correlation, inertial dissipation, profile, and bulk. Of these, the last requires bulk transfer coefficients (i.e., C_{D10N}) to be determined using one of the alternative methods. Also, the profile method, although yielding valuable results over land, has rarely been used successfully over the sea, where the gradients are much weaker. See Dupuis et al. (1995) for recent results using the profile method to estimate heat and water vapor fluxes over the sea.

Of the remaining two methods, the eddy-correlation (EC) method is the most straightforward in that it calculates the flux directly from the covariance of the two time series. For instance, the surface stress is given by Eq. (1) either directly or in spectral form. The EC method has been widely and successfully applied to tower data (e.g., Smith 1980; Large and Pond 1981; Donelan 1990; Smith et al. 1992; Edson et al. 1991), with the latter authors showing the importance of siting the anemometers in a region free of flow distortion effects. Clean towers, however, are restricted to a few coastal locations; the bulk of the global ocean is much more conveniently accessed by ship or buoy. That these latter platforms are nonstationary, however, means that the measured wind components are contaminated by the motion of the sensor and, hence, that eddy correlation calculations may include a substantial, or dominant,

nonturbulent component. It has been estimated (e.g., Donelan 1990) that a 1° error in the mean tilt of an anemometer can result in an EC stress error of 10%. On a ship or buoy, instantaneous anemometer tilt angles can exceed 10°.

Given the difficulties in implementing the eddy correlation method, the inertial dissipation (ID) method has found common usage (e.g., Large and Pond 1981; and Dobson et al. 1994 using ships; or Large and Pond 1981; Smith 1980; Edson et al. 1991; and Smith et al. 1992 from coastal towers). The ID method assumes that the sum of pressure working and transport terms in the kinetic energy balance equation is negligible, resulting in a relationship between friction velocity $u_* = (\tau/\rho)^{1/2}$ and the kinetic energy dissipation rate ϵ , the latter of which can be calculated from the spectrum of u' or w' . The calculation of ϵ uses only the spectral values at high frequencies, which are in the so-called inertial subrange, well above those associated with most platform motions. Thus, the dissipation method is well suited for use on moving platforms, such as ships or aircraft. We emphasize that the ID method, although in common usage, is an approximation. It is subject to the same requirements as the EC method, namely that conditions are steady and homogeneous, and in addition depends on the assumptions that pressure working and transport terms are small or in balance and that the coefficients in the relation are well known. The coefficients depend on atmospheric stratification, which implies an assessment of the turbulent momentum flux and buoyancy.

In order to use the EC method on moving platforms, the complete motion of the platform must be recorded at each time step, and each velocity sample corrected. Early applications of the EC method to ship measurements made the assumption that some or all of the ship motion was negligible. In particular, Mitsuta and Fujitani (1974) neglected the linear accelerations of the ship, while Bradley et al. (1991) neglected all ship motion for measurements made in the Tropics. The early use of inertial platform systems for aircraft led to the development of motion correction algorithms (e.g., Miyake et al. 1970); Fujitani (1985) used a similar system for ship measurements. Recent advances in motion sensing technology mean that it is now feasible to employ the eddy correlation technique on both ships (see Fujitani 1992; or Katsaros et al. 1993) or buoys (Ancitl et al. 1994). Thus, this more accurate calculation method can now be employed in typical oceanic conditions.

The Surface Wave Dynamics Experiment (SWADE) was carried out off the Atlantic coast of the United States over the six months of October 1990 through March 1991 in the area shown in Fig. 1. A complement of buoys—including four National Data Buoy Center (NDBC) 3-m Discus buoys and three meteorological buoys—recorded directional wave spectra and meteorological data in the SWADE area throughout the entire period. In addition, three intensive operating periods (IOPs) of two weeks each were selected for detailed

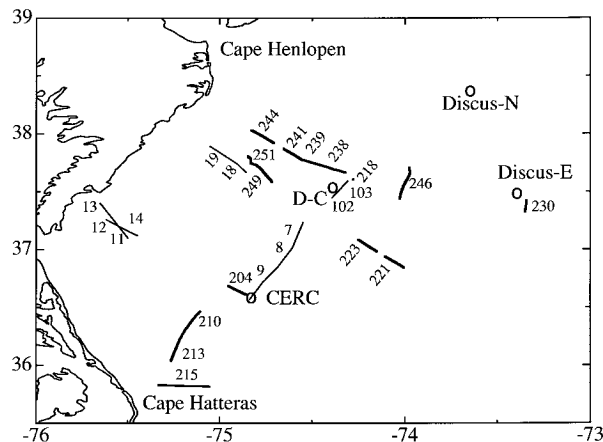


FIG. 1. Chart of the SWADE area showing NDBC 3-m Discus buoys (○). The lines mark the location and track of the *Frederick G. Creed* during the flux runs. The numbers on the graph indicate run numbers. Details of the runs are given in Table 1.

observation and modeling. During the IOPs of January 1991 (IOP2) and February–March 1991 (IOP3), several aircraft plus the 20-m SWATH (small water-plane area, twin hull) Ship *Frederick G. Creed* were deployed. We report here on measurements primarily from the *Creed*, along with supporting data from the NDBC buoys.

3. Shipborne measurements during SWADE

A SWATH ship such as the *Creed* offers minimal surface resistance and is well streamlined so that it

makes an excellent air–sea interaction platform in addition to allowing it to achieve the design goal of high speed operation. The ship, seen in Fig. 2, is 20 m long by 10 m wide, with buoyancy provided by two submerged pontoons that are connected to the superstructure by narrow struts running the length of the ship. Each pontoon holds one of the ship’s engines: cruising speeds of up to 13 m s⁻¹ are possible, although 2–3 m s⁻¹ speeds were more typical during the data gathering runs. High stability in pitch and roll is provided by a system of computer controlled lifting surfaces that protrude from the front and rear of each pontoon.

For the purposes of SWADE, special equipment was installed on the *Creed*. The turbulence and wave sensors employed in this study are described. The 9-m mast installed on the foredeck of the ship—see Fig. 2—held a K-Gill anemometer–vane, a pair of thermocouples, and a Lyman- α humidiometer. The latter instruments were mounted behind a “spray-flinger” for protection from sea salt. The K-Gill anemometer consists of two propellers mounted 45° above and below the horizontal plane (Ataktürk and Katsaros 1989). A motion package consisting of three linear accelerometers, a pitch–roll gyroscope, and a three-axis magnetometer was positioned near the bow of the ship. These sensors measure the full six degrees of motion of the ship (heave, surge, sway, pitch, roll, and yaw).

Analysis of the turbulence data was carried out in blocks of 17 min. Details of the algorithm used to obtain EC estimates of u_* from the measured signals are given

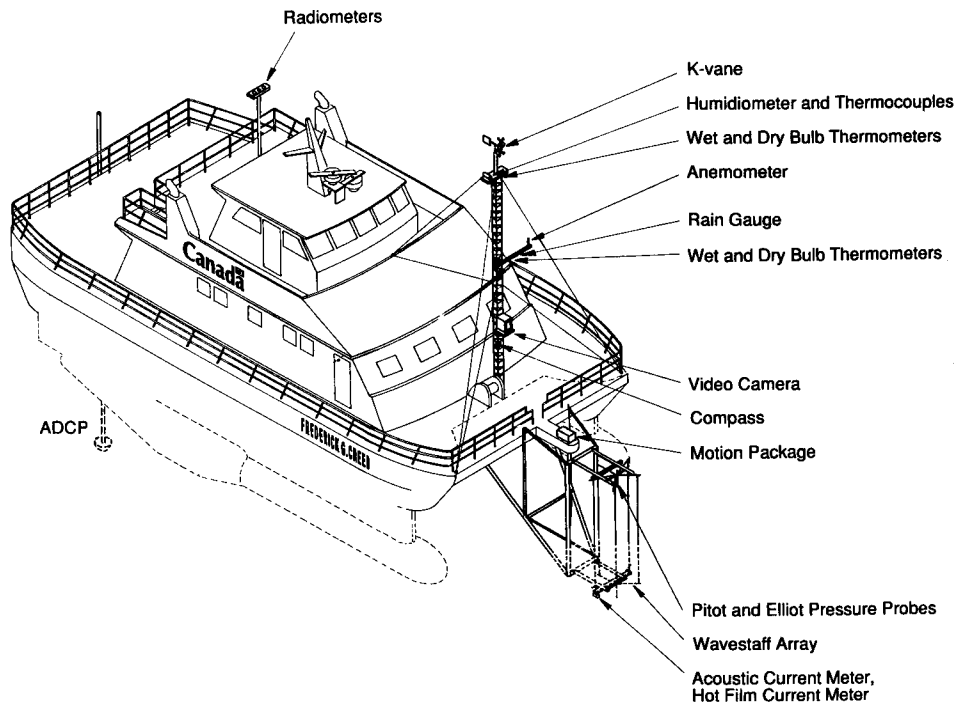


FIG. 2. Illustration of the SWATH Ship *Frederick G. Creed* showing the equipment deployed during SWADE.

by Katsaros et al. (1993); the basic steps are the following:

- Correction for the 5-Hz RC antialiasing filter used during data acquisition.
- Determination of mean (i.e., 17-min average) pitch and roll angles using the surge and sway accelerometers.
- Correction for frequency response of the K-Gill propellers following Hicks (1972). The distance constant for the carbon fibre propellers was determined to be 2.2 m.
- Correction for frequency response of the K-Gill vane following MacCready and Jex (1964). In wind flume tests, the damping coefficient and natural (undamped) wavelength of oscillation for the second-order vane response correction were found to be 0.465 and 7.83 m.
- Computation of the velocity components in the K-Gill reference frame (equivalent to the ship reference frame, SR), following Ataktürk and Katsaros (1989).
- Computation of the velocity components in an earth-referenced (ER) frame, following Anctil et al. (1994). The calculation, performed at each time step, consists of (i) rotating the measured SR velocities into an ER frame, (ii) adding the ER velocity fluctuations of the ship itself, and (iii) accounting for the relative motion between the ship (motion package) and K-Gill.
- Rotation of the ER horizontal and vertical velocities (u and w) so that $\bar{w} = 0$.

In addition to turbulence measurements, the SWATH ship was equipped with an array of wave staffs for estimation of the directional wave spectrum. The retractable array was mounted on a bowsprit about 2 m in front of the bow (4 m ahead of the pontoons), and consisted of either six staffs arranged in a centered pentagon of radius 75 cm (during January and February) or three staffs arranged in a triangle with sides 1.4 m \times 1.4 m \times 2 m (during March). The staffs were 4.5 m long by 0.9-mm diameter Teflon-coated high carbon steel wires, tensioned by strong springs. The wave height time series of the staffs were processed to obtain estimates of directional spectra according to the algorithm of Drennan et al. (1994). The principal steps are as follows:

- Correction for the 5-Hz RC antialiasing filter used during data acquisition.
- Transformation of the ship referenced measurements to earth referenced ones. The calculation, performed at each time step, consists of (i) rotating the measured (SR) elevations into an ER frame, (ii) adding the ER vertical movement of the ship itself, and (iii) accounting for the relative displacement between the ship motion package and wave staffs. This accounts for the unsteady motion of the ship.
- Determination of the Jacobian of the transformation between the intrinsic frequency ω , and the apparent or observed frequency n . The two are different due

to the Doppler shifting of frequencies caused by the steady forward motion of the ship at speed U and are related by $n = \omega + kU \cos\alpha$ where k is the wave-number and α the angle between the wave component and ship heading.

- Estimation of directional wave spectra using a modified maximum likelihood method (MLM); see Drennan et al. (1994). The method uses the wavenumber k , but as discussed by Kats and Spevak (1980) and Drennan et al. (1994), the mapping from ω to k is not one-to-one over the entire domain. Pointing the ship into the wind and assuming that short waves [$k > g(2U \cos\alpha)^{-2}$] do not travel against the wind permits a unique inversion.

Representative spectra are shown in Fig. 3 in polar form and in geophysical coordinates, which is with north at the top and east to the right. The plots show evenly spaced energy contours, with the energy plotted in the direction the waves are traveling.

In a few cases, for example, run 204, directional spectra estimates from the ship were not obtained due to a faulty wave staff. In these cases, spectra from the nearest NDBC 3-m Discus buoy were used. These spectra are calculated from the hourly stored coefficients, each based on 20 minutes of data. Comparisons of the ship and buoy spectra were found by Drennan et al. (1994) to be in good agreement. No wave data are available during runs 11 and 12 due to broken wave staffs and because the ship was near shore at the time, well away from any buoys.

During the data runs, the ship cruised into the wind at speeds of 2–3 m s⁻¹ making both wave and turbulence measurements. Criteria for the selection of runs are that meteorological and wave conditions remain stable during the course of the run; the speed and heading of the ship remain stable; the ship heading be within $\pm 30^\circ$ of the upwind direction; and the mean wind with respect to the ship be greater than 5 m s⁻¹. The first two conditions are dictated by requirements of ergodicity, the third by flow effects, and the fourth by the limitations in the response of the K-Gill anemometer. Since the ship speed into the wind was 2–3 m s⁻¹, this restriction excludes only the wind speed range under 2–3 m s⁻¹.

4. Momentum flux data

The mid-Atlantic coastal region was chosen as the site for the SWADE experiment in part for its proximity to the Gulf Stream and in part for the high likelihood of “interesting” weather. Typical winter conditions consist of alternating cold dry continental and warm humid gulf air masses passing over the region, often with strong frontal zones.

The buoy Discus-East, located at the eastern edge of the SWADE zone, was anticipated to be in the Gulf Stream. In fact, during IOP3, the Gulf Stream meandered well landward of its normal path so both Discus-

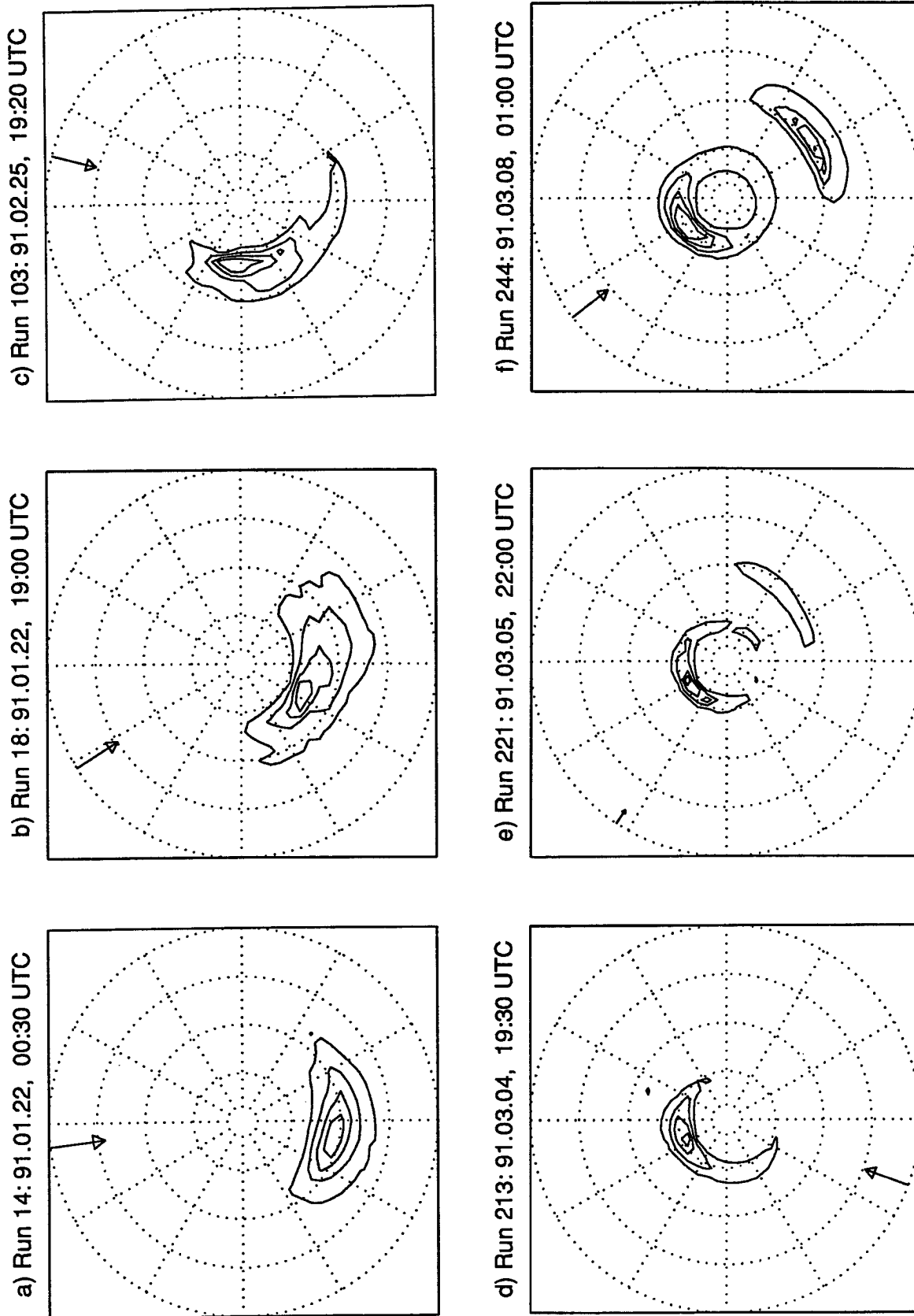


FIG. 3. Sample directional frequency spectra from the *Frederick G. Creed*. The spectra are estimated from wave array measurements based on the algorithm of Drennan et al. (1994). Grid lines are 30° apart with frequencies every 0.1 Hz to a maximum of 0.4 Hz. North appears at the top of the plot, east at the right. The wave energy is shown in the direction of propagation with equally spaced contours normalized to the energy maximum. The average wind appears as an arrow pointing in the direction of the wind with an arrow of length equal to the 0.1-Hz spacing equivalent to a wind speed of 10 m s^{-1} .

E and -C were in either the Gulf Stream or warm core eddies for much of the time. Periods when the *Creed* was in the Gulf Stream are evident from the water temperature column of Table 1. Water temperatures of approximately 20°C contrast with more typical coastal winter water temperatures of 10°C. The water temperatures are obtained by merging bucket, ADCP, ship intake, and daily AVHRR infrared satellite data.¹

The three NDBC Discus buoys North, East, and CERC roughly demarcated the boundaries of the SWADE zone and allow a cross-calibration of the flux and wave measuring capabilities of the 3-m buoys and the SWATH ship. However, although EC flux measurements were made at Discus-North and -Centre (see Anctil et al. 1994), the ship was not at sea at the time, so a cross-comparison of flux data is not possible.

a. Environmental conditions

The data presented here, 126 runs in all, are concentrated in two time periods with very different conditions.

Thirty-six runs were recorded in the four-day time period 19–22 January 1991 during IOP2. Hourly meteorological conditions (5-m wind speed and direction, significant height H_s , air temperature T_a , and atmospheric pressure) for the period as measured by three NDBC 3-m Discus buoys moored in the SWADE area are shown in Fig. 4. At the start of the first data runs (1800 UTC 19 Jan 1991) conditions were near neutral (slightly unstable) with winds blowing from the southeast. Directional spectra during these runs (7–9) show a pure wind sea (period 5 s) building from significant height (taken to be four times the rms surface elevation) of 0.5 m to over 1 m. On 20 January, a low pressure region followed by a cold front passed over the area. The wind veered to NNW and the air temperature gradually dropped from 12° to -4°C as cold air entered the region, resulting in more highly unstable conditions. Hourly directional spectra from the buoys show the old wind sea decaying and a new wind sea dominant by the time ship measurements resumed late on 21 January. Figure 3a shows the directional spectrum measured from the *Creed*. With strong winds, and the sea building to a significant height of 3.5 m near Discus-C, the *Creed* stayed closer to the coast (runs 11–14). By the time of the final set of January runs (18–19), the wind was still strong from the NNW. The effect of the coast line can be seen by the turning of the old sea along the coast Fig. 3b.

A set of five runs (102–103) was made on 25 February 1991 during the first part of IOP3. During these runs, the *Creed* was in the Gulf Stream, experiencing unstable atmospheric conditions. Typical conditions are shown

in Fig. 3c: a wind sea generated by moderate winds from the north with a cross swell from the east. A day later, in similar conditions, the wave staff array was lost during an encounter with a large wave, necessitating a return to port for repairs.

The first week of March 1991 saw the bulk of the *Creed's* data runs. Hourly atmospheric conditions for the 8-day interval as measured by three NDBC 3-m Discus buoys in the SWADE area are shown in Fig. 5. The evolution of the wave field at buoys Discus-North, -Centre, and CERC can be seen in Fig. 6. The figure shows the evolution of the hourly one-dimensional wave spectra with time, with the contours marking energy density in logarithmically spaced intervals.

Conditions over the week can be summarized as follows: For 24 hours from around 1800 UTC 1 March a southerly wind blew at speeds increasing from 2 to 15 m s⁻¹, bringing warm air and leading to stable conditions. During this time a wind sea developed, with H_s at the buoys increasing to between 3.5 and 5 m. Note also the downshifting of the peak frequency as the wave field developed (Fig. 6). During 3 March, the wind shifted to the southwest and decayed somewhat. The wave field was then dominated by a 2–3 m, 9 s, SSE swell (propagating toward 330°). The characteristic increase of the swell frequency over the next 24 hours reflects the arrival of successively slower (higher frequency) components from a distant storm. Early on 4 March the swell veered toward the north (propagating from the south) and intensified; the pattern of increasing frequency is repeated. These swells dominated the SWADE area during most of the SWATH ship runs in March.

At about 1800 UTC 3 March during run 204, the wind shifted briefly to the south-southeast (following swell) and then back to the southwest (cross swell) for much of 4 March (runs 210–213, Fig. 3d). During the night of 4–5 March, a cold front passed through the SWADE area (recorded on the *Creed*, south of CERC buoy at 0620 UTC 5 March). The winds shifted to the northwest and decreased. Runs 221–223 are characterized by light winds, blowing almost directly against the 2–2.5 m swell (Fig. 3e). In Fig. 6 the appearance of the new wind sea (0.2 Hz), first at buoy Discus-North then Discus-Centre, along with the slow decay of the counter swell, can be clearly seen. During the next 18 hours (including run 230), the winds turned to the south-southwest and intensified, bringing warmer air into the SWADE region. These conditions lasted until midday 7 March, with the resident swell increasing in magnitude to 2–3 m. A second cold air outbreak entered the SWADE area late on 7 March, with the wind direction veering to the northwest. Moderate winds blowing against a decaying swell are characteristic of runs 238–251 (Fig. 3f).

b. Methods of analysis

The 12-m measured mean wind speeds were converted to 10-m neutral values, U_{10N} , using the profile

¹ ADCP: acoustic Doppler current profiler, AVHRR: Advanced Very High Resolution Radiometer.

gradient functions of Donelan (1990). Two friction velocity values were calculated by the eddy correlation (u_{*} -EC) and inertial dissipation (u_{*} -ID) methods respectively. The two u_{*} values at 12 m are adjusted to surface values following Donelan (1990). This correction, of at most 4%, accounts for the error in assuming a constant stress layer. For the inertial dissipation values, we first calculate the turbulent kinetic energy (TKE) dissipation rate, ϵ , according to

$$\epsilon = \frac{1}{U_c} (S_u(\omega) \omega^{5/3} / C)^{3/2}, \quad (2)$$

where $S_u(\omega)$ is the frequency spectrum of u' in the inertial subrange where $S_u \propto \omega^{-5/3}$, U_c the mean convection velocity of the turbulent eddies past the anemometer (Taylor's hypothesis is assumed), and C the Kolmogorov constant. Edson et al. (1991) present the various values of C used in the literature, with a range of 0.52 to 0.6, depending on the formulation used in its derivation. We use the value of Large and Pond (1981), that is, $C = 0.55$. Once ϵ is determined, the friction velocity can be found from the assumption that TKE production and dissipation are in balance; namely

$$\frac{\epsilon \kappa z}{u_*^3} = \phi_u \left(\frac{z}{L} \right) - \frac{z}{L}, \quad (3)$$

where the von Kármán constant κ is taken to be 0.4, ϕ_u is the momentum gradient function given by Donelan (1990), z the measurement height above the surface, and L the Monin-Obukhov length. Here L is taken to be

$$L = \frac{u_*^3 T_v}{g \kappa w' T_v'}, \quad (4)$$

where T_v is the virtual temperature, related to temperature T and specific humidity m according to $T_v = T + 0.61Tm$. For each run, a mean value of L was calculated using the time series of the temperature and humidity as measured on the *Creed*.

The significant wave heights were found and a classification of each run was made according to the wave conditions. Four categories are used: pure wind sea (w), and wind sea with either following swell (f), cross swell (x), or counter swell (c). The three swell classifications are defined according to the relative directions of the wind sea and swell as estimated from the directional spectra. Coincident directions within 45° are termed following; opposing directions within 45° , counter; and all others, cross. This is a rough classification. High swells propagating at, say, 60° against a wind sea have a significant "counter" component but are classified as cross-swells. Also, it would be useful to further classify the data by relative magnitude of the swell and wind sea, but we have an insufficiently large sample for making this subclassification. As noted above, during most of the March runs, a strong swell dominated the wind sea.

5. Results

Table 1 provides an overview of the data runs. In Fig. 7a we plot the eddy correlation friction velocity, u_{*} -EC, versus neutral 10-m wind speed, stratifying the data as discussed above. Also shown is the curve summarizing the data of Smith (1980). These results were determined using the EC method on data from a tower off the Nova Scotian coast. Although the curve fits the pure wind sea data subset (27 points) fairly well, especially at lower wind speeds, it underestimates the cross- and counter-swell data by about 50% on average. The number of following-swell cases is too low to warrant further discussion. In Fig. 7b we show a similar graph with u_{*} calculated by the inertial dissipation method. Again, the relation of Smith (1980) fits the pure wind sea data reasonably well (especially at lower winds) but underestimates the cross- and counter-swell data. There is also evidence of additional stratification between these latter sets, with counterswell cases showing larger friction velocities than cross-swell cases.

In Figs. 8a and 8b, a comparison is made between u_{*} -EC and u_{*} -ID. For pure wind sea cases, the two are seen to agree well, with a 9.8% rms difference (with respect to the mean). For cross- and counter-swell conditions, the two methods show an rms difference of 22.7%.

In Fig. 9, we see the drag coefficient $C_{D10N} = u_*^2 / U_{10N}^2$ plotted for the various swell conditions, along with the curve describing the data of Smith. A linear regression to the eddy correlation data pure wind sea case yields the curve

$$C_{D10N} = 10^{-3}(0.1371U_{10N} + 0.0458), \quad (5)$$

which is not significantly different from the fit to the data for pure wind sea with u_{*} evaluated by the inertial dissipation method. When the swell data (cross and counter) are included, the best fit results in the constant drag coefficient $C_{D10N} = 0.0019$. However, this fit is heavily biased by the presence of the eight data points in the upper left corner of Fig. 9 (i.e., low winds, high drag). These data are from runs 221, 223, and 239, conditions of a strong swell running against a light wind. When these data are excluded from the fit, a regression yields

$$C_{D10N} = 10^{-3}(0.07U_{10N} + 0.95). \quad (6)$$

In general, as the wind speed increases, the difference in drag coefficients between the pure wind sea and mixed wind sea/swell datasets decreases, although there is considerable scatter.

6. Discussion

The light wind, high counter-swell data are of considerable interest in that they exhibit drag coefficients up to 3 times higher than would be expected based on the remainder of the dataset. The drag coefficients from

TABLE 1. Data summary. Symbols are U_{12} and U_{10N} : 12-m and neutral 10-m winds speeds respectively, T_a : air temperature, T_w : water temperature, P_{atm} : atmospheric pressure, L : Monin–Obukhov length, $u_* - EC$ and $u_* - ID$: friction velocity via eddy correlation and inertial dissipation respectively, and H_s : significant wave height. The “class” column classifies each run as pure wind sea (w) and wind sea with either following-swell (f), cross-swell (x), or counter-swell (c).

run	date	time UTC	U_{12} [m s ⁻¹]	U_{10N} [m s ⁻¹]	T_a [°C]	T_w [°C]	P_{atm} [mb]	L [m]	$u_* - e.c.$ [m s ⁻¹]	$u_* - i.d.$ [m s ⁻¹]	H_s [m]	class
7-01	1991.01.19	22:01	10.22	10.22	11.16	13.0	1016	-158.4	0.299	0.322	0.82	w
7-03	1991.01.19	22:18	10.10	10.11	11.18	13.0	1016	-155.7	0.378	0.399	0.82	w
7-05	1991.01.19	22:35	10.45	10.44	11.11	13.0	1016	-166.3	0.398	0.377	0.88	w
8-01	1991.01.20	00:15	10.00	10.00	11.02	12.7	1015	-161.0	0.344	0.360	0.93	w
8-03	1991.01.20	00:32	9.97	9.98	10.83	12.7	1015	-148.5	0.358	0.362	0.95	w
8-05	1991.01.20	00:49	9.60	9.63	10.97	12.7	1015	-140.3	0.384	0.375	0.94	w
8-07	1991.01.20	01:15	9.46	9.40	10.91	11.7	1015	-243.2	0.318	0.342	0.95	w
8-09	1991.01.20	01:32	9.01	8.96	10.89	11.7	1015	-210.4	0.316	0.306	0.96	w
9-02	1991.01.20	03:17	8.91	8.84	10.89	11.3	1014	-304.2	0.288	0.326	1.00	w
9-04	1991.01.20	03:34	8.83	8.76	10.88	11.3	1014	-294.0	0.282	0.309	1.02	w
9-06	1991.01.20	03:51	8.46	8.42	10.69	11.3	1014	-216.0	0.257	0.236	1.11	w
9-08	1991.01.20	04:17	8.16	8.18	10.26	11.3	1013	-137.6	0.262	0.278	1.07	w
9-10	1991.01.20	04:34	7.87	7.91	10.21	11.3	1013	-120.5	0.263	0.292	1.02	w
9-12	1991.01.20	04:51	7.33	7.41	9.97	11.3	1013	-85.9	0.226	0.262	1.02	w
9-14	1991.01.20	05:17	6.20	6.38	9.77	11.3	1012	-50.0	0.219	0.220	0.92	w
9-16	1991.01.20	05:34	5.31	5.48	9.69	11.3	1012	-32.2	0.147	0.163	0.82	w
9-18	1991.01.20	05:51	4.80	5.07	9.54	11.3	1012	-16.8	0.145	0.125	0.72	w
11-01	1991.01.21	19:46	13.53	13.40	6.14	8.8	1004	-262.3	0.574	0.520		w
12-01	1991.01.21	20:40	11.48	11.51	5.55	8.8	1005	-137.9	0.458	0.494		w
12-03	1991.01.21	20:57	11.22	11.26	5.60	8.8	1005	-131.2	0.404	0.521		w
13-01	1991.01.21	21:48	10.03	10.16	5.45	8.8	1006	-92.0	0.430	0.357	1.04	w
14-01	1991.01.22	00:07	11.28	11.44	4.80	9.8	1008	-87.4	0.461	0.432	1.57	w
14-03	1991.01.22	00:24	11.24	11.42	4.58	9.8	1008	-83.3	0.463	0.456	1.57	w
14-05	1991.01.22	00:41	11.67	11.84	4.31	9.8	1008	-88.0	0.503	0.532	1.56	w
14-07	1991.01.22	00:58	11.99	12.15	3.98	9.8	1008	-89.8	0.487	0.510	1.63	w
14-09	1991.01.22	01:15	11.86	12.05	3.69	9.8	1008	-83.1	0.511	0.477	1.60	w
14-11	1991.01.22	00:07	11.27	11.51	3.60	9.8	1008	-70.8	0.505	0.525	1.67	w
18-01	1991.01.22	17:40	10.11	10.80	-3.59	9.3	1017	-24.8	0.478	0.590	2.21	x
18-03	1991.01.22	17:57	10.49	11.23	-3.65	9.3	1017	-27.4	0.552	0.482	2.05	x
18-05	1991.01.22	18:14	10.23	10.86	-3.60	9.3	1017	-25.7	0.447	0.433	2.10	x
18-07	1991.01.22	18:31	9.93	10.84	-3.46	9.3	1017	-23.9	0.611	0.463	1.75	x
18-09	1991.01.22	18:48	9.95	10.68	-3.35	9.3	1017	-24.2	0.491	0.448	1.95	x
18-11	1991.01.22	19:05	9.91	10.58	-3.16	9.3	1017	-24.3	0.458	0.534	1.90	x
19-01	1991.01.22	20:16	9.07	9.48	-3.19	9.3	1019	-19.0	0.229	0.454	1.59	f
19-03	1991.01.22	20:33	8.61	9.51	-3.14	9.3	1019	-16.5	0.467	0.364	1.58	f
19-05	1991.01.22	20:50	8.81	9.28	-3.10	9.3	1019	-17.7	0.252	0.390	1.48	f
102-01	1991.02.25	17:10	11.04	11.48	9.62	20.3	1012	-37.6	0.428	0.501	2.46	x
102-03	1991.02.25	17:27	10.66	11.01	9.34	20.3	1012	-33.3	0.304	0.483	2.60	x
102-05	1991.02.25	17:44	10.24	10.82	9.36	20.3	1012	-29.7	0.457	0.415	2.47	x
103-01	1991.02.25	18:59	9.54	10.15	9.20	20.3	1012	-24.2	0.409	0.361	2.59	x
103-03	1991.02.25	19:16	9.12	9.60	9.25	20.3	1012	-21.4	0.293	0.420	2.72	x
204-01	1991.03.03	18:43	10.67	9.64	16.34	10.0	999	71.3	0.333	0.355	2.00	f
204-03	1991.03.03	19:00	8.53	7.19	16.73	10.0	999	37.9	0.255	0.258	2.00	f
204-05	1991.03.03	19:17	8.75	7.21	17.51	10.0	999	36.3	0.283	0.279	2.00	f
204-07	1991.03.03	19:34	9.39	7.96	18.22	10.0	999	39.6	0.286	0.276	2.00	f
204-09	1991.03.03	19:43	9.40	8.00	18.51	10.0	998	38.3	0.255	0.276	2.00	f
204-11	1991.03.03	20:00	9.84	8.25	19.24	10.0	998	39.6	0.315	0.257	2.00	f
204-13	1991.03.03	20:17	10.88	9.37	19.87	10.0	998	48.2	0.356	0.336	2.00	f
210-01	1991.03.04	12:10	13.37	12.72	14.36	11.5	986	308.0	0.539	0.541	2.99	x
210-03	1991.03.04	12:27	12.56	11.77	14.34	11.5	986	261.3	0.604	0.512	3.12	x
210-09	1991.03.04	13:10	13.84	13.23	14.35	12.4	987	533.1	0.609	0.652	3.00	x
210-11	1991.03.04	13:27	14.32	13.75	14.42	12.4	987	563.1	0.594	0.596	3.12	x
210-13	1991.03.04	13:44	14.69	14.15	14.36	12.4	987	626.9	0.597	0.649	3.12	x
211-01	1991.03.04	14:37	14.40	13.92	14.32	13.0	988	993.7	0.584	0.631	2.97	x
211-03	1991.03.04	14:54	13.61	13.19	14.08	13.0	988	1182.4	0.535	0.564	3.15	x
211-05	1991.03.04	15:11	13.42	13.00	14.04	13.0	988	1204.5	0.539	0.566	3.41	x
212-02	1991.03.04	16:38	8.83	8.20	13.02	11.2	989	170.5	0.377	0.324	2.88	x
212-04	1991.03.04	16:55	8.90	8.45	12.93	11.2	989	185.9	0.293	0.338	2.75	x
212-06	1991.03.04	17:12	10.00	9.46	13.11	11.2	989	224.0	0.381	0.404	2.71	x
212-08	1991.03.04	17:29	10.14	9.62	13.15	11.2	989	226.1	0.376	0.399	2.86	x
212-10	1991.03.04	17:46	9.25	8.72	13.15	11.2	989	178.1	0.329	0.349	3.00	x
212-13	1991.03.04	17:30	9.97	9.34	13.53	10.8	989	146.7	0.346	0.369	3.06	x

TABLE 1. (Continued)

run	date	time UTC	U_{12} [m s ⁻¹]	U_{10N} [m s ⁻¹]	T_a [°C]	T_w [°C]	P_{atm} [mb]	L [m]	$u_{*-c.c.}$ [m s ⁻¹]	$u_{*-i.d.}$ [m s ⁻¹]	H_s [m]	class
213-01	1991.03.04	18:56	9.67	9.10	13.47	11.0	989	151.5	0.322	0.362		x
213-03	1991.03.04	19:13	9.00	8.31	13.52	11.0	989	122.6	0.333	0.331	3.17	x
213-05	1991.03.04	19:30	9.79	9.12	13.74	11.0	989	139.4	0.333	0.342	2.72	x
213-07	1991.03.04	19:47	10.40	9.83	13.65	11.0	989	169.3	0.341	0.407	2.93	x
213-09	1991.03.04	19:56	10.80	10.49	12.75	12.0	989	1092.2	0.414	0.466	2.88	x
213-11	1991.03.04	20:13	9.99	9.53	13.58	12.0	989	284.6	0.372	0.375	2.66	x
213-13	1991.03.04	20:30	9.68	9.23	13.54	12.0	989	270.4	0.349	0.353	2.70	x
215-01	1991.03.05	01:00	9.68	9.76	12.06	14.5	995	-109.3	0.423	0.388	3.14	x
215-03	1991.03.05	01:17	10.01	10.07	12.10	14.5	995	-122.4	0.430	0.428	2.68	x
215-05	1991.03.05	01:34	9.01	9.16	11.95	14.5	995	-85.6	0.411	0.362	2.73	x
215-08	1991.03.05	02:00	8.61	8.73	11.93	14.0	996	-94.2	0.401	0.359	2.64	x
215-10	1991.03.05	02:17	8.82	8.82	11.68	14.0	996	-92.9	0.000	0.326	2.84	x
215-12	1991.03.05	02:34	8.85	8.99	11.57	14.0	996	-86.3	0.406	0.339	2.65	x
215-14	1991.03.05	02:51	8.52	8.67	11.71	14.0	996	-81.7	0.375	0.337	2.56	x
215-16	1991.03.05	03:08	8.79	8.91	11.75	14.0	996	-91.3	0.397	0.362	2.39	x
215-18	1991.03.05	03:25	8.51	8.68	11.72	14.0	996	-83.0	0.442	0.393	2.13	x
215-20	1991.03.05	03:42	8.76	8.90	11.61	14.0	996	-86.4	0.390	0.341	2.02	x
218-03	1991.03.05	15:17	7.28	7.94	7.17	16.5	1010	-13.9	0.309	0.362	2.50	c
221-01	1991.03.05	21:09	3.32	4.79	11.00	18.8	1012	-1.9	0.286	0.171	2.54	c
221-03	1991.03.05	21:26	3.35	4.51	11.05	18.8	1012	-2.0	0.228	0.160	2.68	c
221-05	1991.03.05	21:43	2.73	3.51	11.07	18.8	1012	-1.3	0.132		2.45	c
221-07	1991.03.05	22:00	2.74	3.98	11.18	18.8	1012	-1.3	0.214	0.122	2.28	c
223-01	1991.03.05	23:09	3.72	4.91	11.47	19.5	1013	-2.3	0.247	0.144	1.86	c
223-03	1991.03.05	23:26	3.85	4.51	11.58	19.5	1013	-2.5	0.142	0.162	1.94	c
223-05	1991.03.05	23:43	4.17	5.13	11.55	19.5	1013	-3.0	0.219	0.188	1.85	c
223-07	1991.03.06	00:00	4.07	4.81	11.56	19.5	1013	-2.9	0.167	0.182	1.74	c
230-01	1991.03.06	17:17	6.95	7.41	16.02	19.6	1012	-27.3	0.343	0.328	1.93	x
230-03	1991.03.06	17:34	7.50	7.92	16.08	19.6	1012	-33.9	0.367	0.322	2.04	x
230-05	1991.03.06	17:51	7.95	8.22	16.16	19.6	1012	-40.6	0.282	0.312	2.05	x
230-07	1991.03.06	18:08	8.07	8.39	16.27	19.6	1012	-43.5	0.363	0.351	2.13	x
238-01	1991.03.07	19:08	7.34	7.68	12.10	15.0	999	-41.4	0.360	0.346	2.35	c
238-03	1991.03.07	19:25	7.97	8.23	11.87	15.0	999	-48.4	0.318	0.320	2.48	c
238-05	1991.03.07	19:42	6.97	7.36	11.66	15.0	999	-31.8	0.325	0.256		c
239-01	1991.03.07	20:32	4.93	5.39	11.24	12.5	1001	-21.2	0.281	0.216	2.26	c
239-03	1991.03.07	20:49	4.58	5.04	11.16	12.5	1001	-17.1	0.248	0.193	2.02	c
239-05	1991.03.07	21:06	5.04	5.48	11.24	12.5	1001	-21.9	0.275	0.241	2.21	c
239-07	1991.03.07	21:23	5.20	5.52	11.26	12.5	1001	-33.4	0.281	0.250	2.27	c
241-01	1991.03.07	22:29	7.39	7.05	10.99	10.0	1003	354.7	0.294	0.305	2.09	c
241-03	1991.03.07	22:46	6.78	6.52	10.76	10.0	1003	756.1	0.304	0.305	2.05	c
241-05	1991.03.07	23:03	6.69	6.54	10.59	10.0	1003	-2008.8	0.260	0.326	2.02	c
244-01	1991.03.08	00:33	9.23	9.04	9.45	9.2	1004	-906.8	0.384	0.422	1.87	c
244-03	1991.03.08	00:50	9.66	9.48	9.25	9.2	1004	-618.7	0.400	0.440	1.90	c
244-05	1991.03.08	01:07	8.86	8.78	9.05	9.2	1004	-339.4	0.403	0.372	1.88	c
244-07	1991.03.08	01:24	8.99	8.90	8.88	9.2	1004	-305.3	0.359	0.349	1.86	c
246-01	1991.03.08	10:25	8.46	9.14	6.69	19.4	1014	-15.1	0.332	0.405	2.56	c
246-05	1991.03.08	10:59	9.29	10.13	6.30	19.4	1014	-18.9	0.475	0.452	2.47	c
246-07	1991.03.08	11:16	8.97	9.87	6.08	19.4	1014	-16.9	0.472	0.428	2.49	c
246-09	1991.03.08	11:34	9.24	10.12	5.84	19.5	1015	-17.8	0.484	0.450	2.55	c
246-11	1991.03.08	11:51	9.29	9.81	5.54	19.5	1015	-17.9	0.283	0.426	2.49	c
246-13	1991.03.08	12:08	9.95	10.72	5.47	19.5	1015	-21.4	0.476	0.471	2.77	c
246-15	1991.03.08	12:25	10.66	11.37	5.37	19.5	1015	-25.8	0.499	0.534	2.56	c
246-18	1991.03.08	12:49	10.97	11.53	4.95	18.8	1015	-28.6	0.431	0.469	2.64	c
246-20	1991.03.08	13:06	10.79	11.39	4.75	18.8	1015	-27.0	0.435	0.469	2.56	c
249-01	1991.03.08	21:23	7.57	7.95	5.60	10.0	1015	-32.3	0.321	0.313	1.44	c
249-03	1991.03.08	21:40	7.47	7.81	5.69	10.0	1015	-31.6	0.287	0.318	1.43	c
249-05	1991.03.08	21:57	7.91	8.24	5.82	10.0	1015	-37.8	0.327	0.320	1.51	c
249-07	1991.03.08	22:14	6.96	7.30	5.99	10.0	1015	-28.0	0.254	0.328	1.41	c
249-09	1991.03.08	22:31	7.15	7.48	6.08	10.0	1015	-30.9	0.270	0.281	1.43	c
249-11	1991.03.08	22:48	6.66	7.03	6.19	10.0	1015	-26.1	0.262	0.293	1.40	c
249-13	1991.03.08	23:05	6.08	6.44	6.20	10.0	1015	-20.7	0.222	0.249	1.31	c
250-02	1991.03.08	23:44	6.33	6.62	6.61	10.1	1017	-24.3	0.201	0.256	1.23	c
250-05	1991.03.09	00:06	6.91	7.17	6.85	10.3	1017	-31.1	0.220	0.231	1.15	c
250-08	1991.03.09	00:33	7.66	7.89	6.86	10.2	1017	-41.9	0.246	0.283	1.19	c
251-01	1991.03.09	01:00	7.81	8.04	6.80	10.0	1018	-45.5	0.280	0.322	1.20	c

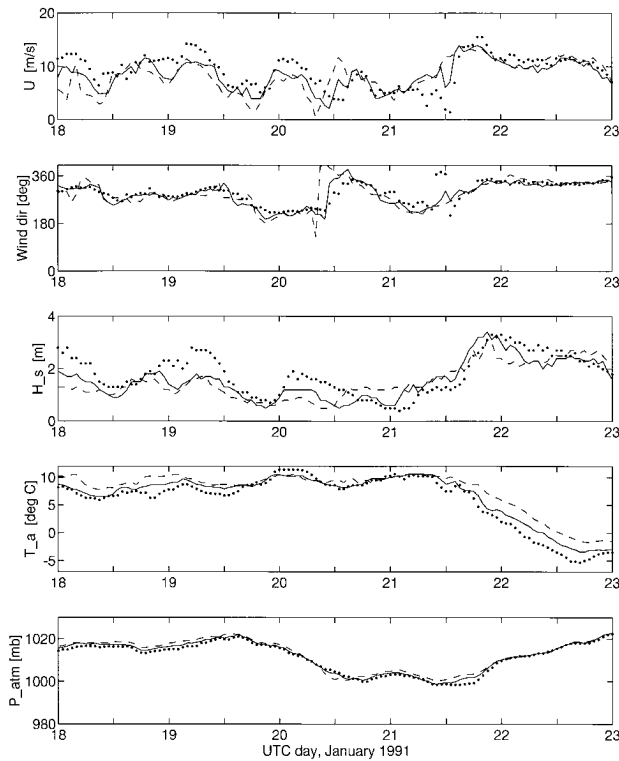


FIG. 4. Hourly meteorological data for 18–23 January 1991 from the NDBC 3-m Discus buoys Discus-Centre (—), CERC (---), and Discus-North (.....). The five panels show (a) wind speed, (b) wind direction, (c) significant wave height, (d) air temperature, and (e) atmospheric pressure.

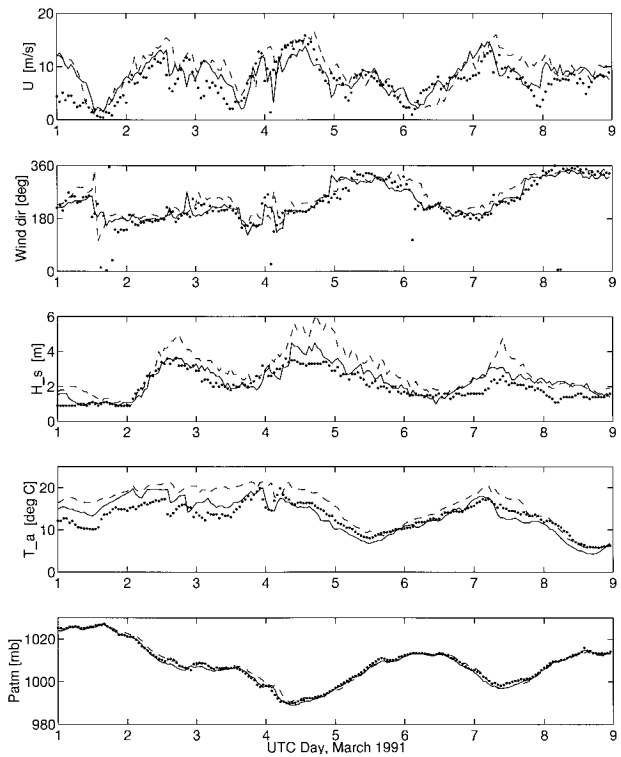


FIG. 5. As in Fig. 4 but for 1–9 March 1991 with Discus-Centre (—), Discus-East (---), and CERC (.....).

these 12 cases (runs 221, 223, 239), with a mean of 0.0024 (0.00077 std dev), are significantly different at the 95% confidence level from the C_D prediction for pure wind sea data. In as much as these cases also include some of the largest anomalies between EC and ID methods, with EC drag coefficients 45% higher in the mean, the question of the reliability of these data must be asked. Although the wind speeds are relatively low, they are well within the acceptable range for the K-Gill anemometer: the addition of the ship speed ensured that the flow through the anemometer met the 5 m s^{-1} minimum mean wind speed criterion. The individual time series of wind speed through each propeller were also checked for low values to ensure that the propellers did not stall. Any questionable data were rejected.

A second possible source of error is in the motion correction algorithm itself. However, in similar wave conditions, with higher wind speeds (runs 238, 241, and 244), the drag coefficient difference between EC and ID methods is reduced to under 2%. Given that the ship responds to the wave field in both cases, it is difficult to attribute the differences to errors in the motion correction algorithm. Instead, it is likely that the differences are due to the inability of the ID method to account for the effects of low-frequency swell components in the

wave field on the momentum flux. An alternative explanation has been offered recently by Dupuis et al. (1995). They proposed that the sum of the pressure working and transport terms in the kinetic energy balance equation may not be zero, as assumed in (3), but is in fact a function of stability.

Additional SWADE measurements, coincident with those of the SWATH ship, support the results presented above. During IOP-3 the NASA/Ames Research Center C-130B aircraft, equipped with radar scatterometers operating at Ku- and C-bands (the Jet Propulsion Laboratory NUSCAT and the University of Massachusetts C-SCAT, respectively) made frequent overflights of the SWADE area (see Nghiem et al. 1995). Under high-wave, light-wind conditions during SWATH ship runs 221 and 223, the backscatter was significantly enhanced over the high-wave, moderate-wind conditions of SWATH runs 241 and 244. Nghiem et al. (1995) investigated possible causes for the enhancement and concluded that increased wind stress was the likely candidate.

7. Conclusions

The transfer of momentum between wind and sea is generally parameterized in terms of wind speed and atmospheric stratification (stability) only. During the Surface Wave Dynamics Experiment, we developed a sys-

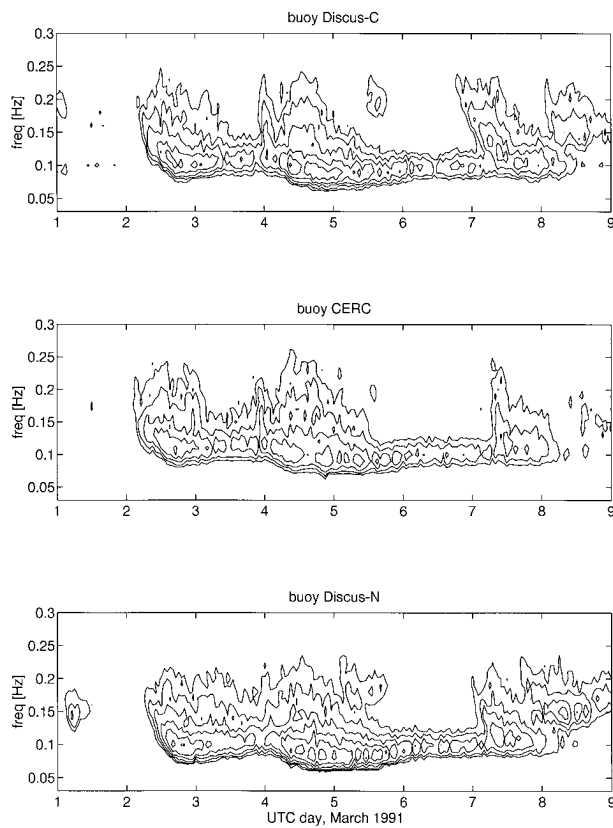


FIG. 6. Hourly one-dimensional surface elevation frequency spectra for 1–9 March 1991 from the NDBC 3-m Discus buoys (a) Discus-Centre, (b) CERC, and (c) Discus-North. The contour lines represent energy density in logarithmic spacing.

tem for the direct measurement of the air–sea fluxes (via eddy correlation) and directional wave spectra from a ship at sea (Katsaros et al. 1993; Drennan et al. 1994). This development has allowed us to explore the effect of wind waves and swell in modifying the transfer of momentum. Since the measurements yield the fundamental quantity $\overline{u'w'}$ directly, the effect of nonequilibrium wave fields such as swell propagating at various directions in relation to the wind direction can be assessed.

For cases of equilibrium pure wind sea, excellent agreement between eddy correlation and inertial dissipation estimates of u_* was obtained. This correspondence was much less evident when swell was present. The inertial dissipation method depends on the assumptions of steady state and similarity of the cascade of energy from scales of input to scales of dissipation. The presence of swell leads to a narrowbanded energy transfer (input) in addition to the broadband self-similar transfer due to roughness of the shorter wind sea spectrum. Because of this, we suggest that the traditional inertial dissipation method is not suitable for estimating the momentum transfer in nonequilibrium wave conditions.

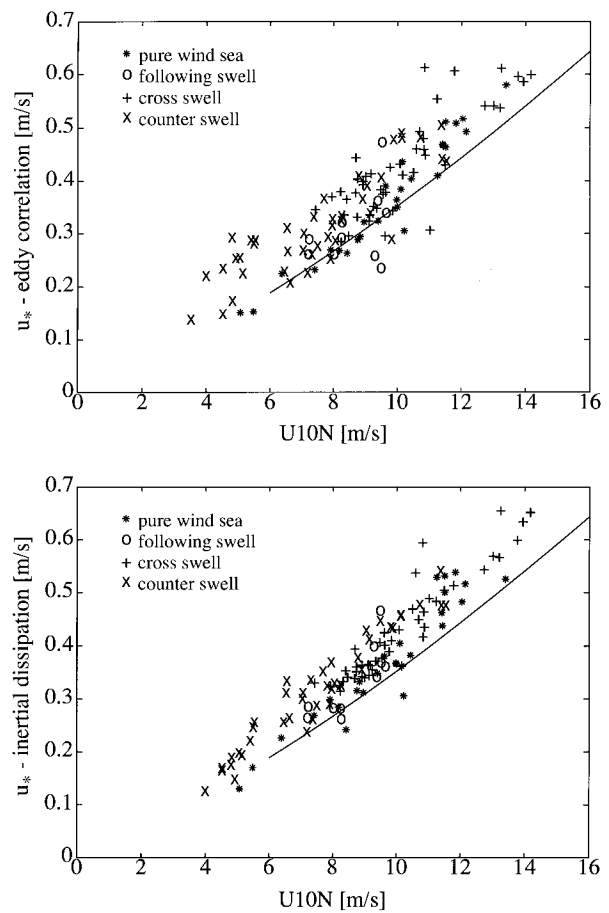


FIG. 7. Plot of friction velocity u_* versus 10-m neutral wind speed for u_* determined by (a) the eddy correlation method and (b) by inertial dissipation. The line in each plot shows the relation of Smith (1980).

The eddy correlation method yields a clear picture of drag coefficient anomalies (i.e., deviations from pure wind sea cases) for cases of well-defined swell combined with wind sea. Counter-swell, propagating against the wind, leads to larger drag coefficients than are encountered in the pure wind sea cases. This dataset, unique in having high-resolution wave directional spectra as well as direct flux measurements, clearly shows that nonequilibrium wave fields strongly affect the air–sea momentum coupling. There are at least two ways in which swell may modify the wind stress: by direct interaction with the air flow, the swell may accept momentum from or deliver it to the atmosphere; by causing a change in the spectral distribution of the components of the wind sea, which are the principal roughness elements (e.g., Donelan 1987). Ultimately, one would like to be able to calculate the wind stress given the full wavenumber directional spectrum of surface elevation and the wind at some reference height in the boundary layer. However, most of the stress is carried by short gravity waves (Donelan 1997) and field measurements of the wavenumber directional spectrum of these waves

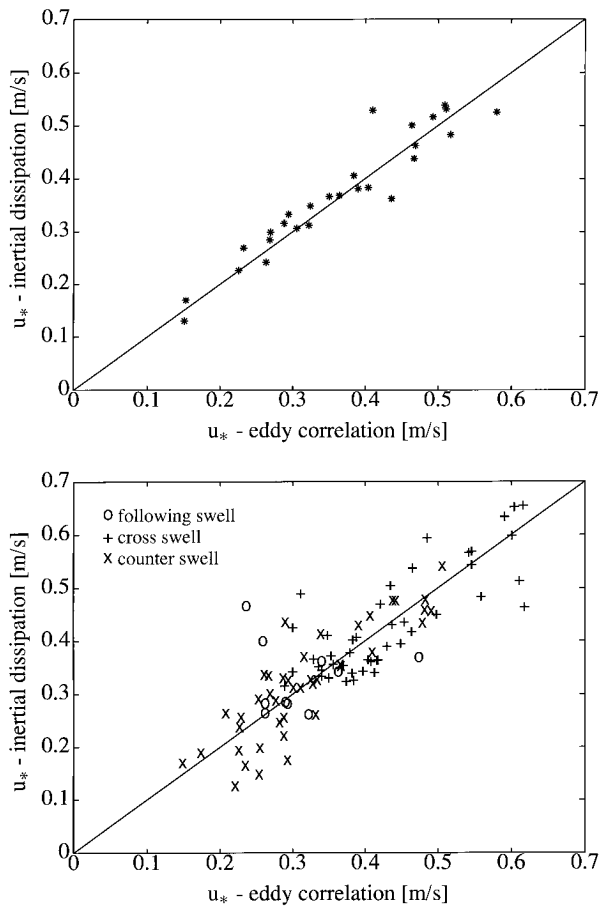


FIG. 8. Comparison of friction velocity u_* as calculated by the eddy correlation and inertial dissipation methods, for (a) only pure wind sea data and (b) mixed wind sea and swell data.

are rare, and likely to remain so for some time. We are continuing to seek accurate parametric descriptions of wind seas and the modulation of wind seas by swell, with a view toward a systematic calculation of the momentum transfer between air and sea for arbitrary conditions. Such formulations would find use in operational wave models and coupled atmosphere–ocean models.

Acknowledgments. We gratefully acknowledge support from the U.S. Office of Naval Research through Grants N0014-94-1-0629 and N0014-88-J-1028 to the National Water Research Institute and N0014-89-1785 to the University of Washington. Support for the use of the SWATH ship was provided by the Office of Naval Research, the National Aeronautics and Space Administration, the Coastal Engineering Research Center of the U.S. Army, Environment Canada, and the Canadian Department of Fisheries and Oceans. We thank Capt. S. Bodman and the crew of the *Frederick G. Creed*, along with fellow scientists C. Flagg, K. Howard, and E. Terray for their many contributions to the work.

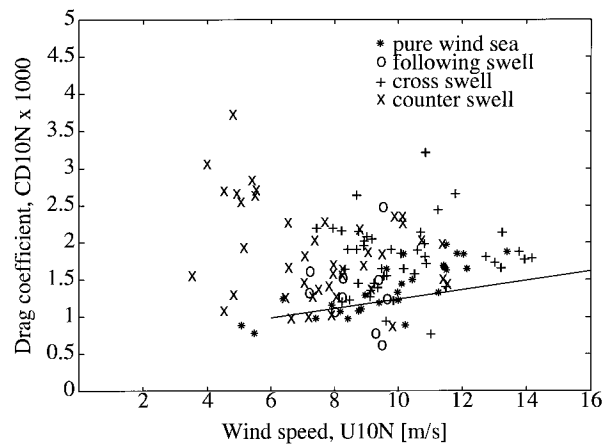


FIG. 9. Ten-meter neutral drag coefficient C_{D10N} versus 10-m neutral wind speed for eddy correlation data and four types of sea state, as shown. The pure wind sea relation of Smith (1980) is indicated with a solid line.

REFERENCES

- Ancil, F., M. A. Donelan, W. M. Drennan, and H. C. Graber, 1994: Eddy correlation measurements of air–sea fluxes from a Discus buoy. *J. Atmos. Oceanic Technol.*, **11**, 1144–1150.
- Ataktürk, S. S., and K. B. Katsaros, 1989: The K-Gill: A twin propeller–vane anemometer for measurements of atmospheric turbulence. *J. Atmos. Oceanic Technol.*, **6**, 509–515.
- Bradley, E. F., P. A. Copping, and J. S. Geoffrey, 1991: Measurements of sensible and latent heat flux in the western equatorial Pacific Ocean. *J. Geophys. Res.*, **96**, 3375–3389.
- Dobson, F. W., S. D. Smith, and R. J. Anderson, 1994: Measuring the relationship between wind stress and sea state in the open ocean in the presence of swell. *Atmos.–Ocean*, **32**, 237–256.
- Donelan, M. A., 1987: The effect of swell on the growth of wind waves. *Johns Hopkins APL Tech. Dig.*, **8**, 18–23.
- , 1990: Air–sea interaction. *The Sea*, B. LéMehauté and D. Hanes, Eds., Vol. 9A, Wiley, 239–292.
- , 1997: Air–water exchange processes. *Physical Limnology*, J. Imberger, Ed., *Coastal Estuar. Studies*, Amer. Geophys. Union, in press.
- , F. W. Dobson, S. D. Smith, and R. J. Anderson, 1993: On the dependence of sea surface roughness on wave development. *J. Phys. Oceanogr.*, **23**, 2143–2149.
- Drennan, W. M., M. A. Donelan, N. Madsen, K. B. Katsaros, E. A. Terray, and C. N. Flagg, 1994: Directional wave spectra from a Swath ship at sea. *J. Atmos. Oceanic Technol.*, **11**, 1109–1116.
- Dupuis, H., A. Weill, K. B. Katsaros, and P. K. Taylor, 1995: Turbulent heat fluxes by profile and inertial dissipation methods: Analysis of the atmospheric surface layer from shipboard measurements during the SOFIA/ASTEX and SEMAPHORE experiments. *Ann. Geophys.*, **13**, 1065–1074.
- Edson, J. B., C. W. Fairall, P. G. Mestayer, and S. E. Larsen, 1991: A study of the inertial-dissipation method for computing air–sea fluxes. *J. Geophys. Res.*, **96**, 10 689–10 711.
- Fujitani, T., 1985: Method of turbulent flux measurement on a ship by using a stable platform system. *Pap. Meteor. Geophys.*, **36**, 157–170.
- , 1992: Turbulent transport mechanism in the surface layer over the tropical ocean. *J. Meteor. Soc. Japan*, **70**, 795–811.
- Hicks, B. B., 1972: Propeller anemometers as sensors of atmospheric turbulence. *Bound.-Layer Meteor.*, **3**, 214–228.
- Kats, A. V., and I. S. Spevak, 1980: Reconstruction of the sea-wave spectra from measurements of moving sensors. *Izv. Acad. Sci. USSR, Atmos. Oceanic Phys.*, **16**, 194–200.
- Katsaros, K. B., M. A. Donelan, and W. M. Drennan, 1993: Flux

- measurements from a Swath ship in SWADE. *J. Mar. Syst.*, **4**, 117–132.
- Large, W. G., and S. Pond, 1981: Open ocean momentum flux measurements in moderate to strong winds. *J. Phys. Oceanogr.*, **11**, 324–336.
- MacCready, P. B., and H. R. Jex, 1964: Response characteristics and meteorological utilization of propeller and vane wind sensors. *J. Appl. Meteor.*, **3**, 182–193.
- Mitsuta, Y., and T. Fujitani, 1974: Direct measurement of turbulent fluxes on a cruising ship. *Bound.-Layer Meteor.*, **6**, 203–217.
- Miyake, M., M. A. Donelan, and Y. Mitsuta, 1970: Airborne measurements of turbulent fluxes. *J. Geophys. Res.*, **75**, 4506–4518.
- Nghiem, S. V., F. K. Li, S. H. Lou, G. Neumann, R. E. McIntosh, S. C. Carson, J. C. Carswell, E. J. Walsh, M. A. Donelan, and W. M. Drennan, 1995: Observations on ocean radar backscatter Ku and C bands in the presence of large waves during the Surface Wave Dynamics Experiment. *IEEE Trans. Geosci. Remote Sens.*, **33**, 708–721.
- Pierson, W. J., Jr, 1983: The measurement of synoptic scale wind over the ocean. *J. Geophys. Res.*, **88**, 1683–1708.
- Smith, S. D., 1980: Wind stress and heat flux over the ocean in gale force winds. *J. Phys. Oceanogr.*, **10**, 709–726.
- , R. J. Anderson, W. A. Oost, C. Kraan, N. Maat, J. deCosmo, K. B. Katsaros, K. L. Davidson, K. Bumke, L. Hasse, and H. M. Chadwick, 1992: Sea surface wind stress and drag coefficients: The HEXOS results. *Bound.-Layer Meteor.*, **60**, 109–142.